EPJ Web of Conferences **182**, 02019 (2018) https://doi.org/10.1051/epjconf/201818202019
ICNFP 2017

Relaxation to equilibrium in relativistic heavy ion collisions

L. Bravina[1,a] and E. Zabrodin[1,2,3]

[1] *Department of Physics, University of Oslo, PB 1048 Blindern, Oslo, Norway*
[2] *Skobeltsyn Institute of Nuclear Physics, Moscow State University, RU-119991 Moscow, Russia*
[3] *National Research Nuclear University "MEPhI" (Moscow Engineering Physics Institute), Kashirskoe highway 31, Moscow, RU-115409, Russia*

Abstract. Relaxation to equilibrium of hot and dense matter produced in central area of relativistic heavy ion collisions at energies ranging from several AGeV to hundreds AGeV is studied within two Monte Carlo transport models. The analysis was performed for three different areas: (i) fixed cubic cell with volume $V = 125\,\mathrm{fm}^3$, (ii) fixed asymmetric cell with volume $V = 4 \times 4 \times 1 = 16\,\mathrm{fm}^3$, and (iii) expanding cell. In the last case the cell volume follows the growth of the area with uniformly distributed energy. To check whether or not the system is equilibrated, its hadron yields and their energy spectra are compared with those of the statistical model of ideal hadron gas. For all cells and for all collision energies it was found that the matter in the cell was approaching the equilibrium state. The higher the collision energy, the shorter the time of equilibration. The equilibration phase lasts about 10 - 20 fm/c, after that the matter becomes very dilute and the thermal contact between hadrons is lost. Equation of state is well fitted to linear dependence $P/\varepsilon = a = c_s^2$, where the square of the sonic velocity c_s^2 increases from 0.12 at $E_{lab} = 11.6\,\mathrm{AGeV}$ to 0.145 at $E_{lab} = 160\,\mathrm{AGeV}$. The characteristic kinks observed in the $T - \mu_B$ phase diagrams are linked to inelastic freeze-out in the expanding fireball.

1 Introduction

In 1997-98 the just developed Ultra-relativistic Molecular Dynamics (UrQMD) model [1, 2] has been tested for different colliding systems at various energies. Obtained results were confronted to the available experimental data, and new signals were suggested. One of the ideas, strongly supported by Walter Greiner, was to employ the new microscopic transport model to check the relaxation of hot and dense partonic matter produced in a relativistic heavy ion collision to the equilibrium. Note that the hypothesis of equilibrium in nuclear reactions at ultrarelativistic energies was (and still is) an *ad hoc* assumption to validate the application of equilibrium relativistic hydrodynamics [3–5].

The strategy was as follows. Central collisions of heavy ions, such as Au+Au or Pb+Pb, were considered at energies varying from AGS ($E_{lab} = 11.6\,\mathrm{AGeV}$) [6] up to SPS ($E_{lab} = 160\,\mathrm{AGeV}$) [7–9]) and RHIC ($\sqrt{s} = 130\,\mathrm{GeV}$ and $200\,\mathrm{GeV}$) [10, 11]. The central cubic cell with volume $V = 5 \times 5 \times 5\ fm^3 = 125\,\mathrm{fm}^3$ was chosen to investigate the local equilibration of matter. Why local? - It became obvious after study the evolution of the baryon densities in central A+A collisions, as displayed in Fig. 1 for lead-lead collisions at SPS energy, that the baryonic matter is non-homogeneously

[a] e-mail: larissa.bravina@fys.uio.no

distributed even between the remnants of two nuclei. Therefore, global equilibrium is unlikely to occur, whereas the local equilibrium in the central cell is not ruled out.

Because of the expansion of the fireball, the energy density, baryon density, and particle composition in the cell are changing all the time. To decide whether or not the matter is in local equilibrium, or very close to it, one has to compare the conditions in the cell, i.e. particle yields and energy spectra, either with those of an infinite nuclear matter or with the calculations according to statistical model (SM) of an ideal hadron gas. Both scenarios were realized. The developed procedure is quite thorough. Firstly, the necessary prerequisites of the kinetic equilibrium are checked. It implies that the pressure in the cell is isotropic in longitudinal and transverse directions, i.e. no strong collective flows in a particular direction. After that one has to compare hadron abundances in the cell and their energy spectra with those obtained from the SM calculations with the same values of energy density, baryon density, and strangeness density. If the results will be close to each other, say, within 10% of accuracy, this would imply that the matter in the cell is in the vicinity of the state of thermal and chemical equilibrium. This scheme was applied to heavy ion collisions at various c.m. energies in [6–12]. Results of the calculations in the central cell were compared also to those of the infinite matter, modeled by the box with periodic boundary conditions [13], in [14]. Finally, the analysis was modified further to trace the expansion of the area of homogeneity, where the energy density was uniformly distributed within the considered coarse-grained volume, see [15–18]. Main results of our investigations are presented below.

The paper is organized as follows. Brief description of the statistical model of an ideal hadron gas is given in Sect. 2. Section 3 presents the study of the pre-equilibrium stage. We also have checked the hypothesis that the equilibrium in a small cell might set in earlier compared the larger one. In Sect. 4 the relaxation of matter to thermal and chemical equilibrium in two microscopic models, ultra-relativistic quantum molecular dynamics and quark-gluon string model (QGSM), is studied at energies from $E_{lab} = 11.6$ AGeV up to $E_{lab} = 160$ AGeV. The scheme with the cells of increasing sizes is also considered. Finally, conclusions are drawn in Sect. 5.

2 Statistical model of ideal hadron gas

The model assumes that the system of hadrons is in a complete chemical and thermal equilibrium. This means that the spectra of all hadronic species are characterized by a unique temperature T. Thermal equilibrium is maintained by (quasi)elastic collisions. Inelastic collisions may occur also, but they must be fully reversible to not violate the condition of detailed balance. Then, all characteristics of the system of hadrons can be obtained via the moments of the distribution functions (in system of natural units, $\hbar = c = k_{\rm B} = 1$)

$$f(p_i, m_i) = \left[\exp\left(\frac{E_i - \mu_i}{T}\right)\right]^{-1} \quad , \tag{1}$$

$$E_i^2 = p_i^2 + m_i^2 \quad , \tag{2}$$

$$\mu_i = \mu_B B_i + \mu_S S_i \quad , \tag{3}$$

where E_i, p_i, and μ_i are energy, momentum, and mass of the hadronic specie i, respectively, B_i and S_i are its baryon and strangeness content, and μ_B and μ_S are the baryon and the strangeness chemical potentials. One has to know just three parameters, namely T, μ_B, and μ_S, to determine particle number

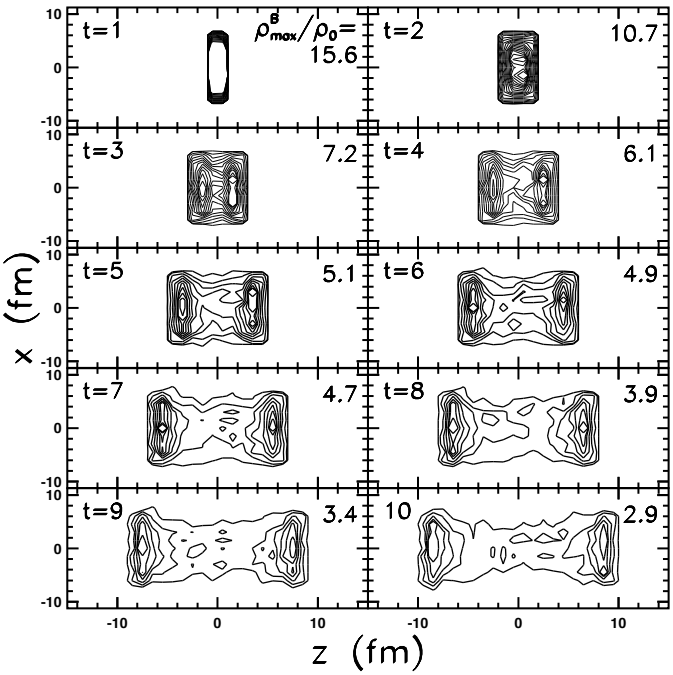

Figure 1. Time evolution of baryon density in XZ-plane in central Pb+Pb collisions at E_{lab} = 160 AGeV in UrQMD calculations.

density n_i, energy density ε_i, and partial pressure P_i, respectively:

$$n_i = \frac{g_i}{2\pi^2}\int_0^\infty f(p,m_i)p^2dp \quad , \tag{4}$$

$$\varepsilon_i = \frac{g_i}{2\pi^2}\int_0^\infty f(p,m_i)E_ip^2dp \quad , \tag{5}$$

$$P_i = \frac{g_i}{2\pi^2}\int_0^\infty f(p,m_i)\,\frac{p^2}{3E_i}\,p^2dp \quad , \tag{6}$$

where g_i is the spin-isospin degeneracy factor.

To calculate the entropy density s_i in the SM one can use either the Gibbs identity

$$s_i = \left(\varepsilon_i + P_i - \mu_B\rho_{B_i} - \mu_S\rho_{S_i}\right)/T \quad , \tag{7}$$

with ρ_{B_i} and ρ_{S_I} being the density of baryon number and strangeness, respectively, or directly via the distribution function

$$s_i = -\frac{g_i}{2\pi^2} \int_0^\infty f(p, m_i) \, [\ln f(p, m_i) - 1] \, p^2 dp \quad . \tag{8}$$

From the analysis of the cell conditions in microscopic calculations, however, one can extract total energy density, ε^{mic}, net baryon density, ρ_B^{mic}, and net strangeness density, ρ_S^{mic}. To find the three basic parameters, i.e. T, μ_B, μ_S, we have to insert the values of $\varepsilon^{mic}, \rho_B^{mic}$, and ρ_S^{mic} determined at time t into a system of highly non-linear equations

$$\varepsilon^{mic} = \sum_i \varepsilon_i^{\rm SM}(T, \mu_B, \mu_S) \quad , \tag{9}$$

$$\rho_B^{mic} = \sum_i B_i \cdot n_i^{\rm SM}(T, \mu_B, \mu_S) \quad , \tag{10}$$

$$\rho_S^{mic} = \sum_i S_i \cdot n_i^{\rm SM}(T, \mu_B, \mu_S) \quad . \tag{11}$$

To compare "apples to apples" the number of degrees of freedom, i.e. particles and antiparticles, in the SM should be equivalent to that of the employed microscopic model. After determining of T, μ_B, μ_S one can directly compare particle abundances and energy spectra provided by the microscopic and macroscopic models to decide whether or not the statistical equilibrium is reached in the cell.

3 Stage of pre-equilibrium in microscopic models

In what follows we employ two different microscopic models, UrQMD [1, 2] and QGSM [19–21]. Both models are designed to describe hadronic, hadron-nucleus, and nucleus-nucleus collisions in a broad energy range. In the UrQMD model the longitudinal excitation of strings is employed, and the string masses arise from momentum transfer. In the QGSM model the string masses appear due to the color exchange mechanism, and strings are stretched between the constituents belonging to different hadrons. Also, the fragmentation functions which determine the energy, momentum, and type of the hadrons produced during the string decay, are different in the models. Both UrQMD and QGSM utilize the experimentally available information, such as hadron cross sections, resonance widths and decay modes. If this information is lacking, the one-boson exchange model, detailed balance considerations and isospin symmetry conditions are employed. The propagation of particles is governed by Hamilton equation of motion, and both models use the concept of hadronic cascade for the description of hA and $A + A$ interactions. Due to the uncertainty principle newly produced particles can interact further only after a certain *formation time*. Only hadrons containing the valence quarks can interact immediately with the reduced cross section $\sigma = \sigma_{qN}$. The Pauli principle is taken into account via the blocking of the final state, if the outgoing phase space is occupied.

When generating the heavy ion collision, we have to wait until the two Lorentz-contracted nuclei would have passed through each other. This time, $t^{cross} = 2R/(\gamma_{c.m.} v_{c.m.})$, decreases from 5.5 fm/$c$ at $E_{lab} = 11.6$ AGeV to 2.9 fm/c and 1.45 fm/c at $E_{lab} = 40$ AGeV and 160 AGeV, respectively. Then, the necessary conditions of the pre-equilibrium stage imply the absence of significant velocity gradients in the cell or rather the velocity isotropy in $x-$, $y-$, and $z-$directions. Average velocities of baryons and mesons in longitudinal and transverse directions for all three reactions are displayed in Fig. 2. To avoid the situation with two fluxes moving in opposite directions and, therefore, canceling each other, the calculations are performed just for 1/8 of the cell with coordinates 0 fm$\leq (x, y, z) \leq$2.5 fm. The

average velocity $< v_z >$ dominates over its transverse counterpart, $< v_T >$ at $t = t^{cross}$. Then $< v_z >$ quickly drops, and both velocity components start to converge at $t \approx 10$fm/c.

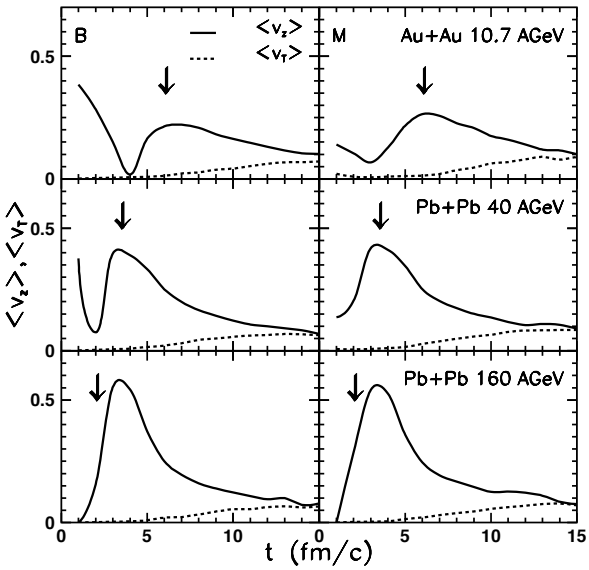

Figure 2. Evolution of average longitudinal $< v_z >$ and transverse $< v_T >$ velocity of baryons (left windows) and mesons (right windows) in asymmetric cell with $0 \leq \{x, y, z\} \leq 2.5$ fm in UrQMD calculations of central heavy ion collisions at bombarding energies 11.6 AGeV (upper row), 40 AGeV (middle row) and 160 AGeV (bottom row), respectively.

Another method is to check the isotropy of pressure in $x-$, $y-$, and $z-$directions. According to the virial theorem, diagonal elements of the pressure tensor are calculated as

$$P^{mic}_{\{x,y,z\}} = \frac{1}{V} \sum_i \frac{p^2_{i,\{x,y,z\}}}{3E_i} \quad , \tag{12}$$

where V is the cell volume, E_i is the energy of the i-th hadron, and $p_{i,(x,y,z)}$ is its momentum in $x-, y-, z-$ direction, respectively. Pressures calculated in the microscopic models in $z-$ and $x-$directions in central Au+Au collisions at six different bombarding energies from $E_{lab} = 11.6$ AGeV to 158 AGeV are compared in Fig. 3 with the total pressures P determined both microscopically and from the SM calculations. In contrast to the case with transverse and longitudinal velocities, pressures in three directions become isotropic already at $t = 2 - 5$ fm/c after beginning of the collision. Note also the good agreement between the microscopic and macroscopic calculations for a period of about $10-15$ fm/c. After $20-25$ fm/c the hadronic matter in the cell is so dilute that the (quasi)elastic collisions cannot maintain thermal equilibrium anymore.

We also have checked the hypothesis that string-hadronic matter in the smaller cell would equilibrate much faster compared to that in the larger volume. Figure 4 depicts the calculations of pressure

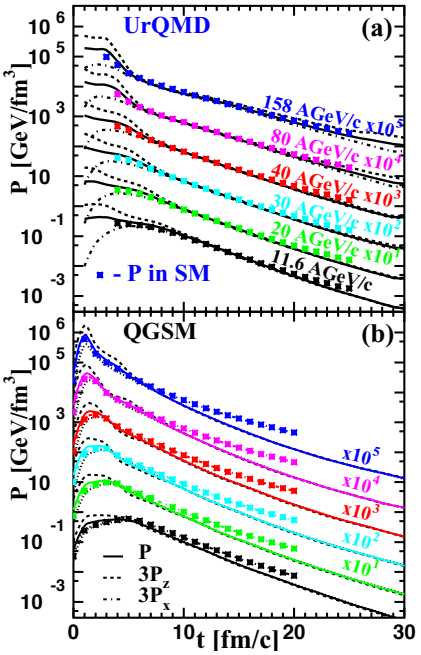

Figure 3. (a) Time evolution of pressure (solid lines) and triple pressure components in longitudinal (dashed lines) and transverse (dash-dotted lines) directions in the central cell of Au+Au collisions at energies from 11.6 AGeV to 160 AGeV in UrQMD calculations. Symbols indicate the SM calculations. (b) The same as (a) but for QGSM calculations.

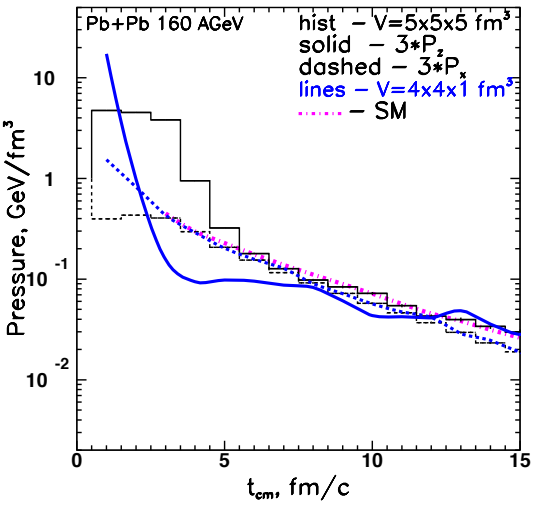

Figure 4. The same as Fig. 3 but for Pb+Pb collisions at 160 AGeV in UrQMD calculations for big cell with $V = 5\times5\times5$ fm^3 (black curves) and for small cell with $V = 4\times4\times1$ fm^3 (blue curves). Magenta dotted line indicates SM calculations.

in longitudinal and transverse directions in Pb+Pb central collisions at $E_{lab} = 160$ AGeV for two cells: one is our "standard" $5\times5\times5$ fm^3 one, whereas the sizes of the other cell are reduced, especially in the longitudinal direction, to $4\times4\times1$ fm^3. The comparison shows that the reduction of the cell size does not lead automatically to early equilibration time. As was first mentioned in [7], the baryon velocity distributions are equilibrated much earlier than that of mesons because of the larger formation time for non-leading particles, mainly pions.

4 Relaxation to equilibrium

4.1 Chemical and thermal equilibrium in $V = 125 fm^3$ cell

The energy spectra $dN/4\pi pEdE$ of most abundant hadron species produced in central Pb+Pb collisions at $E_{lab} = 40$ AGeV at $t = 10$ fm/c and 13 fm/c are shown in Fig. 5. Comparison of the slopes of microscopic spectra with the slopes calculated within the SM demonstrates a fair agreement within 7% of accuracy. Thus, the matter in the cell is very close to thermal equilibrium.

Time evolution of hadron yields in Au+Au collisions at 11.6 AGeV is displayed in Fig. 6. Here we present not only the total yields of particles in microscopic model calculations compared to those

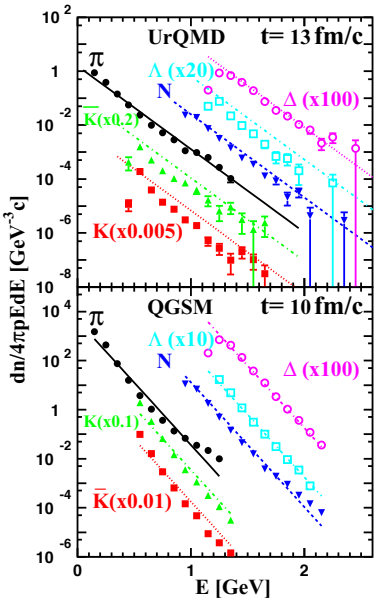

Figure 5. (Upper plot) Energy spectra of main hadron species in UrQMD calculations of Au+Au at 40 AGeV for central cell with $V = 125$ fm^3 at $t = 13$ fm/c. Lines indicate the fit to Boltzmann distribution. (Bottom plot) The same as upper one but for QGSM calculations at $t = 10$ fm/c.

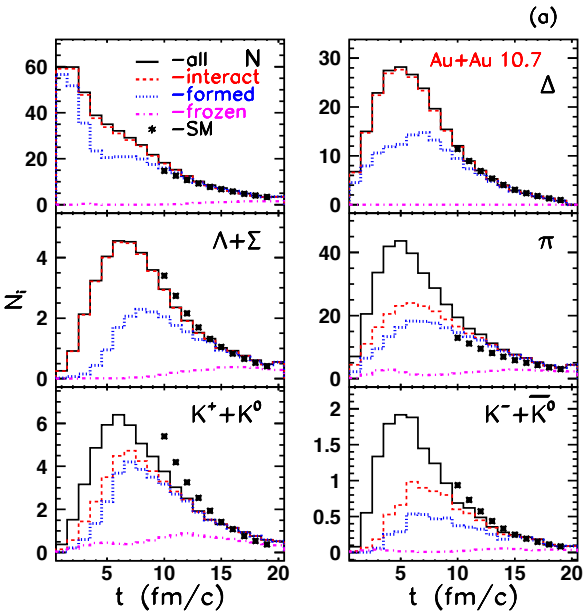

Figure 6. Evolution of particle abundances (histograms) in central cell with $V = 125$ fm^3 in UrQMD calculations of Au+Au collisions at $E_{lab} = 11.6$ AGeV. Asterisks denote the SM results. Also shown are fractions of interacting (dashed), formed (dotted), and already frozen (dash-dotted) hadrons.

in the SM, but subdivided the microscopically calculated spectra into yields of (i) still interacting particles, (ii) formed particles, and (iii) frozen particles. Recall that leading baryons can interact immediately after the collision, although with the reduced cross sections, whereas mesons produced in the collision can interact only after certain formation time determined from the uncertainty principle. Fraction of frozen particles consists of hadrons already decoupled from the system. We see that at $t \geq 10$ fm/c abundances of hadrons provided by microscopic model calculations almost coincide with those calculated within the statistical model.

The situation is changed a bit with increasing collision energy. Figure 7 shows the abundances of the same hadron species as in Fig. 6 but for Pb+Pb collisions at $E_{lab} = 160$ AGeV. All hadron yields, except the pion one, agree well with the SM spectra. Pion yields are overpredicted. To clarify the case, we plot onto the cell yields, calculated microscopically, the abundances of hadron species obtained for the equilibrated infinite nuclear matter within the same microscopic model. The latter was simulated by a box with periodic boundary conditions [13, 14]. One can see that the cell and the box calculations are close to each other already at $t \approx 2 - 3$ fm/c. The discrepancy between the cell/box and the SM calculations arises because of (i) lack of inverse many-particle reactions and (ii) finite lifetime of resonances. This means that matter in the cell reaches steady state rather than the SM equilibrium [9].

4.2 Equation of state

Isentropic expansion of hot and dense matter is an important postulate of the hydrodynamic theory put forward by Landau in 1953 [3]. Can we check it? - The cell is an open system and, therefore, its entropy density drops during the fireball expansion. We can, however, check the conservation of entropy density per baryon. The ratio s/ρ_B is depicted in Fig. 8. Both employed microscopic models indicate that the expanding matter maintains this ratio in the cell at constant level during the equilibrium phase. This fact strongly supports the application of hydrodynamics for the description of ultrarelativistic heavy ion collisions.

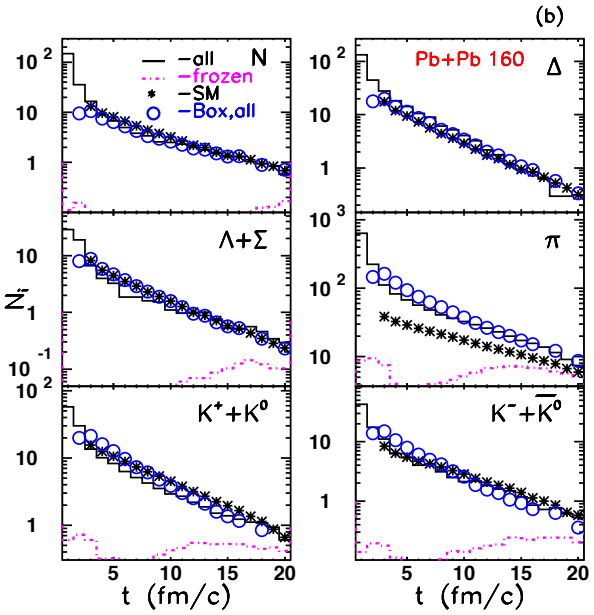

Figure 7. The same as Fig. 6 but for Pb+Pb collisions at E_{lab} = 160 AGeV. Calculations for central cell are also compared to box calculations (open circles).

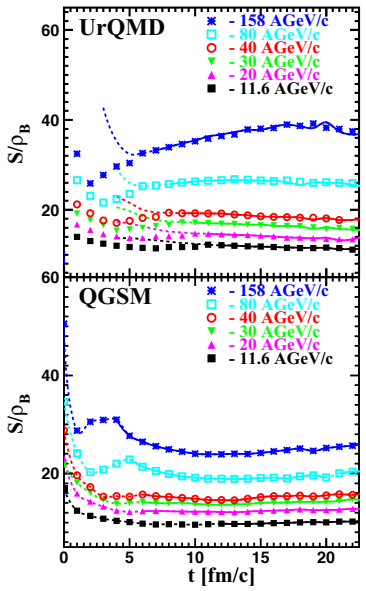

Figure 8. Entropy per baryon ratio vs t in central cell with volume V = 125 fm^3 in UrQMD (upper plot) and QGSM (bottom plot) calculations of central heavy ion collisions at different energies.

The equation of state (EOS) links pressure and energy of the system. Time evolution of the dependencies $P(\varepsilon)$ in central heavy ion collisions for six different bombarding energies from the interval 11.6 AGeV $\leq E_{lab} \leq$ 160 AGeV is displayed in Fig. 9. In both models these dependencies are remarkably linear indicating that the EOS for all energies has a simple form $P = a\varepsilon$, where $\sqrt{a} = c_s$ is the sonic velocity in medium. The slope parameter a is changing from $a = 0.12$ at $E_{lab} = 11.6$ AGeV to $a = 0.145$ at $E_{lab} = 160$ AGeV. Recall, that Landau used in his hydrodynamical model [3, 4] the EOS of ultrarelativistic gas of particles, $P = \varepsilon/3$. Later on this result was revised. It was shown that the presence of resonances reduced the speed of sound up to 1/7 [22]. From the analysis of elliptic flow, PHENIX collaboration estimated the sonic velocity as $c_s^2 = 0.12 \pm 0.03$ [23] in Au+Au collisions at $\sqrt{s} = 200$ AGeV. Both estimates are very close to our results. Note also that both microscopic models

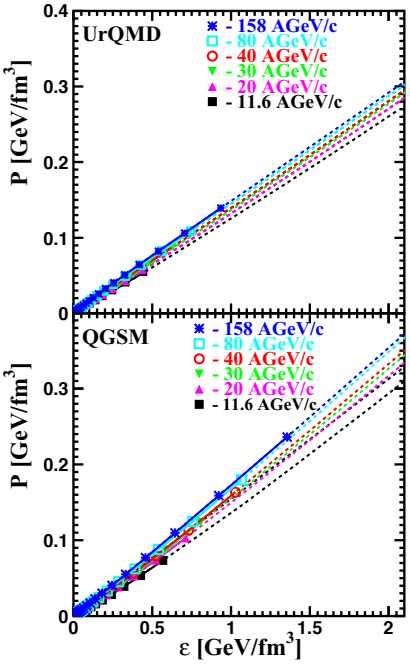

Figure 9. Time evolution of the pressure vs. energy density in the central cell with volume $V = 125\,\mathrm{fm}^3$ in UrQMD (upper plot) and QGSM (bottom plot) calculations of Au+Au collisions at six different energies. Symbols are related to equilibrated matter calculations with the time step $\Delta t = 1$ fm/c.

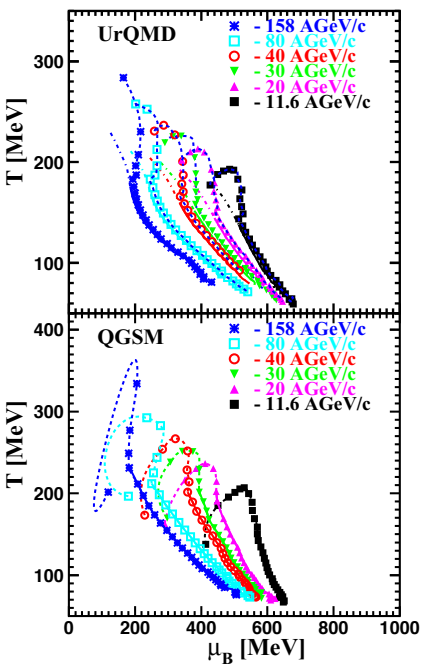

Figure 10. The same as 9 but for $T - \mu_B$ plane. Symbols and dashed curves present the evolution in the cell with increasing volume, whereas dash-dotted and solid curves are related to the fixed-volume cell.

indicate significant deceleration of the c_s^2 increase with rising energy E after $E_{lab} = 40$ AGeV. The sonic velocity is almost the same for heavy ion collisions at SPS and at RHIC energies [10].

4.3 Expanding cell

.

In addition to "small" ($V = 4 \times 4 \times 1$ fm^3) and "big" ($V = 5 \times 5 \times 5$ fm^3) cells of fixed volume, we applied also the scheme where the volume of the cell could expand. The method is as follows. The central area of heavy ion collisions is subdivided into a rather small cells with volume $V = 0.5 \times 0.5 \times 0.5$ fm^3 each. Then, if at a certain time the energy density in the inner cell is the same (within 10% of accuracy limit) as the energy density of the neighbor cells, which form an outer layer of the inner cell, the volume checked for the fulfillment of the equilibrium criteria is enlarged. The next outer layer of small cells is tested, and so forth. Thus, we are somehow following the expanding area of homogeneously distributed energy. This analysis is more accurate compared to that with the cell with fixed volume $V = 125$ fm^3, where energy density can be non-uniformly distributed, especially at the early stage of the heavy ion collision.

The time evolution of the temperature and baryon chemical potential in the central cell for all six energies in question is shown in Fig. 10. Here the symbols connected by the dashed curves

represent the results obtained from the analysis of expanding cells, whereas dash-dotted curves show the evolution of T and μ_B extracted for the fixed-volume cells. During the pre-equilibrium stage the two sets of the obtained parameters are quite different. After beginning of the inelastic freeze-out, however, both methods provide the same results. Therefore the kinks, clearly seen in the $T(\mu_B)$ distributions in Fig. 10, arise in the transport model calculations because of the inelastic freeze-out and not the quark-hadron phase transition, like in some theoretical models [24–26]. It is interesting to note that after the chemical freeze-out temperature depends almost linearly on the baryo-chemical potential for all energies, see Fig. 10. This linear dependence $T = \alpha\mu$, $\alpha = const$ leads to an important consequence. It is possible to show [17] that at $\mu = 0$ the evolution of energy density ε and entropy density s proceeds, respectively, as

$$\frac{\varepsilon}{\varepsilon_0} = \left(\frac{T}{T_0}\right)^{\frac{1+a}{a}} , \tag{13}$$

$$\frac{s}{s_0} = \left(\frac{T}{T_0}\right)^{\frac{1}{a}} , \tag{14}$$

where $a = c_s^2$. In case of non-zero chemical potential the corresponding expressions are a bit more complex

$$\frac{\varepsilon}{\varepsilon_0} = \left(\frac{b\,T+\mu}{b\,T_0+\mu_0}\right)^{\frac{a+1}{a}} , \tag{15}$$

$$\frac{s}{s_0} = \left(\frac{b\,T+\mu}{b\,T_0+\mu_0}\right)^{\frac{1}{a}} , \tag{16}$$

if the expansion of matter in the cell proceeds isentropically with respect to the baryon density, $s/\rho_B = b = const$. Inserting $T = \alpha\mu$ in the last two equations, one regains Eqs. (13)-(14), i.e. evolution of energy and entropy densities is similar to the case with $\mu = 0$.

5 Conclusions

The main conclusion of our study is that two microscopic transport models, UrQMD and QGSM, based on different mechanisms of string excitation and string fragmentation, indicate relaxation of hot and dense nuclear matter, produced in central heavy ion collisions at 11.6 AGeV $\leq E_{lab} \leq$ 160 AGeV, to chemical and thermal equilibrium. The higher the collision energy, the shorter the equilibration time.

The equilibrium state first emerges at t = 8-10 fm/c after beginning of the collision and lasts about 10-15 fm/c. After that time the matter in the cell is very dilute and (quasi)elastic collisions can no longer maintain thermal equilibrium in it. - It looks a bit strange that equilibration in the fireball sets in quite late. However, many distributions, such as EOS-plot or entropy-per-baryon ratio, as well as comparison of the cell calculations with the corresponding box ones, indicate that the state of quasi-equilibrium can be reached already at $t \approx 3-4$ fm/c. In this sense our work supports the results of [27], where it was shown that under a certain conditions the hydrodynamic description can be applicable to systems which are not in local equilibrium. Thus, extremely early equilibration may not be a necessary pre-requisite of the hydrodynamic models [28].

The matter in the central cell expands almost isentropically with constant entropy per baryon ratio. Its EOS is well described by linear dependence $P = c_s^2\varepsilon$, where the speed of sound rises from $c_s^2 = 0.12$ at $E_{lab} = 11.6$ AGeV to 0.14 at $E_{lab} = 40$ AGeV and then slowly increases to 0.145 at

SPS (E_{lab} = 160 AGeV) and RHIC ($\sqrt{s}$ = 200 GeV) energies. The distinct kink seen in $T - \mu_B$ (and also in $T - \mu_S$) phase diagram arises in microscopic calculations for the expanding zone of uniformly distributed energy because of the inelastic freeze-out.

Acknowledgements

The fruitful discussions with M. Bleicher, L. Csernai, I. Mishustin and H. Stöcker are gratefully acknowledged. This work was supported in parts by the Norwegian Research Council (NFR) under grant No. 255253/F50 - “CERN Heavy Ion Theory", and by the Norwegian Centre for International Cooperation in Education (SIU) under grants “CPEA-LT-2016/10094 - From Strong Interacting Matter to Dark Matter" and “UTF-2016-long-term/10076 - Training of Bachelor, Master and PhD Students Specialised in High Energy Physics".

References

[1] S.A. Bass *et al.*, Prog. Part. Nucl. Phys. **41**, 255 (1998)
[2] M. Bleicher *et al.*, J. Phys. **G25**, 1859 (1999)
[3] L.D. Landau, Izv. Akad. Nauk SSSR, Ser. Fiz. **17**, 51 (1953) 51 (in Russian)
[4] S.Z. Belenkij and L.D. Landau, Nuovo Cimento Suppl. **3**, 15 (1956)
[5] H. Stoecker and W. Greiner, Phys. Rept. **137**, 277 (1986)
[6] L.V. Bravina *et al.*, Phys. Lett. **B434**, 379 (1998)
[7] L.V. Bravina *et al.*, J. Phys. **G25**, 351 (1999)
[8] L.V. Bravina *et al.*, Phys. Rev. **C60**, 024904 (1999)
[9] L.V. Bravina *et al.*, Nucl. Phys. **A661**, 600 (1999)
[10] L.V. Bravina *et al.*, Phys. Rev. **C63**, 064902 (2001)
[11] L.V. Bravina *et al.*, J. Phys. **G27**, 421 (2001)
[12] L.V. Bravina *et al.*, Nucl. Phys. **A698**, 383c (2002)
[13] M. Belkacem *et al.*, Phys. Rev. **C58**, 1727 (1998)
[14] L.V. Bravina *et al.*, Phys. Rev. **C62**, 064906 (2000)
[15] L.V. Bravina *et al.*, J. Phys. **G32**, S213 (2006)
[16] L.V. Bravina *et al.*, Int. J. Mod. Phys. **E16**, 777 (2007)
[17] L.V. Bravina *et al.*, Phys. Rev. **C78**, 014907 (2008)
[18] L.V. Bravina *et al.*, J. Phys. **G36**, 064065 (2009)
[19] N.S. Amelin and L.V. Bravina, Sov. J. Nucl. Phys. **51**, 133 (1990)
[20] N.S. Amelin *et al.*, Phys. Rev. **C47**, 2299 (1993)
[21] J. Bleibel, L.V. Bravina, E.E. Zabrodin, Phys. Rev. **D93**, 114012 (2016)
[22] E. Shuryak, Sov. J. Nucl. Phys. **16**, 220 (1973)
[23] A. Adare *et al.* (PHENIX Collaboration), Phys. Rev. Lett. **98**, 162301 (2007)
[24] S. Ejiri, F. Karsch, E. Laermann, C. Schmidt, Phys. Rev. **D73**, 054506 (2006)
[25] A. Khvorostukhin *et al.*, Nucl. Phys. **A791**, 180 (2007)
[26] C. Herold *et al.*, Nucl. Phys. **A925**, 14 (2014)
[27] Ph. Mota, T. Kodama, R.D. de Souza, J. Takahashi, Eur. Phys. J. **A48**, 165 (2012)
[28] Yu.M. Sinyukov, *private communication*